 CMES, vol.6, no.5, pp.453-476, 2004

A Cell Method (CM) Code for Modeling the Pullout Test Step-wise

E. Ferretti[1]

Abstract: The Cell Method (CM) code with automatic remeshing for crack propagation analysis [Ferretti (2003)] is here used for modeling the pullout test. Particular emphasis is given to the analysis in the Mohr-Coulomb plane, since previous numerical models were not decisive in describing failure mechanism in pullout tests. The interpretations of experimental and analytical studies vary widely, and none of the existing explanations offer a complete description of the progressive failure of the concrete medium [Yener (1994)]. Nor do most existing interpretations appear to be totally compatible with the experimental evidence. Analysis of the failure mechanism for the pullout test requires a failure criterion accurately describing crack initiation in tension loading. The Mohr-Coulomb criterion of the first code [Ferretti (2003)] has therefore been abandoned in favor of a more realistic criterion for the tensile state of stress, the Leon criterion. The failure analysis has been performed for several ratios between the counter pressure diameter and the stem length (Fig. 1). Moreover, the complete crack path has been obtained for the geometry of the Lok-test. The evolving state of stress-strain for the Lok-test is also provided. The identification of the directions of principal stress completes the stress analysis. Modeling is performed both on the concrete specimen and on the steel insert, showing how the CM can easily handle domains with several materials.

keyword: Cell Method, automatic remeshing, failure mechanism analysis, Mixed Mode propagation.

1 The pullout test procedure

The pullout test is a nondestructive test procedure which has been suggested by many as an in-place testing procedure alternative to testing field-cast cylinders in the laboratory. The test procedure involves pulling out an anchor plate embedded in concrete with the aid of a tensile jack. During application, a test bolt, consisting of a stem and a circular steel disc, is mounted inside the form (Fig. 1(a)). After curing the concrete, the form is stripped, and the stem is unscrewed. At the time of testing, a rod having a slightly smaller diameter than the stem is screwed into the disc and a cylindrical counter-pressure is mounted (Fig. 1(b)). The rod is loaded by a pullout force until failure, where a small piece of concrete can be punched out if sufficient displacement of the rod is applied.

Requirements for the testing configuration are given in ASTM C 900. The embedment depths (that is, the stem length) and head diameter must be equal, but there is no requirement on the magnitude of these dimensions. Commercial inserts have embedment depths about 25 to 30 mm. The inner diameter of the reaction ring can be any size between 2.0 and 2.4 times the insert-head diameter. This means that the apex angle of the conic frustum defined by the insert-head diameter and the inside diameter of the reaction ring (2α in Fig. 1) can vary between 54 and 70 deg. The test apparatus and procedure for the Danish version of the pullout test, the Lok-Test, are illustrated in Fig. 1 [Ottosen (1981)]. This geometry has been proposed by Kierkegaard-Hansen [Kierkegaard-Hansen (1975)].

The standard pullout test is limited to use in new constructions because the inserts have to be embedded into fresh concrete. However, other types of pullout test configurations are available for existing constructions [Mailhot, Bisaillon, Carette and Malhotra (1979); Chabowski and Bryden-Smith (1980); Petersen (1984); Domone and Castro (1987)]. These typically involve drilling a hole and inserting an expanding anchorage device that will engage in the concrete and cause fracture in the concrete when extracted. These techniques are still under development and have not been standardized as ASTM tests methods.

Extensive field investigations on pullout test have been conducted in Europe, Canada, and the United States. A detailed summary on relevant works can be found in

[1] DISTART – Scienza delle Costruzioni, Alma Mater Studiorum – University of Bologna, ITALY.

Yener and Chen (1984). All laboratory tests indicate that the failure surface is trumpet shaped (Fig. 2). The large diameter of the fragment is determined by the inner diameter of the reaction ring, and the small diameter is determined by the insert-head diameter.

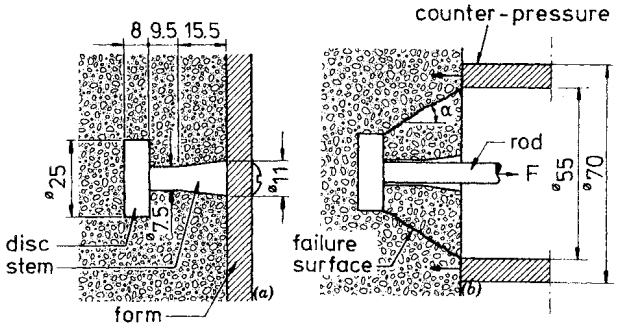

Figure 1 : Application and configuration of Lok-Test (all dimensions are in millimeters)

Figure 2 : Shape of the extracted concrete portion

It was found that the pullout force can be linearly related to the compressive strength measured from standard cylinders or cubes [Yener (1994)]. This relationship is not significantly affected by variations in water-cement ratio, type, shape and size of aggregates up to 40 mm maximum aggregate size, type of cement, curing conditions (water cured, cured in air and maltreated), curing time, admixtures, flyash, and air content. Only the use of lightweight aggregates produces a significantly differ correlation [Petersen (1997)]. Most of the existing hypotheses seem then to describe the behavior of concrete in pullout tests through a uniaxial phenomenon. In spite of that, there has been a considerable amount of controversy regarding the property of concrete that is actually measured in pullout tests [Yener (1994)]. It is not clear whether tension, compression, shear, or punching shear strength of concrete is measured, and what constitutes the physical mechanism of failure. Past tests, confirmed by theoretical considerations based on plastic failure of concrete, have shown that the pullout force essentially depends upon compressive strength only for angles $\alpha = 30^\circ \div 35^\circ$ [Bocca (1984)]. For angles greater than 45° it depends instead, by a constant proportionality, mostly upon tensile strength.

2 State of the art on the pullout modeling

Even if the existence of multiaxial states of stress in pullout tests is recognized in literature, the attribution of the failure process to a uniaxial strength persists.

The available analytical studies on the structural behavior and failure mode of concrete in a pullout test can be summarized as follows:-

Rigid-plasticity analysis. In 1976, Jensen and Bræstrup used the rigid-ideal plasticity theory on an extracted section of concrete assumed to be a truncated cone, with the failure plane running from the outer periphery of the disk toward the inner periphery of the supporting ring (Fig. 3).

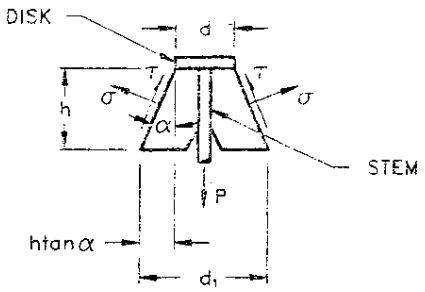

Figure 3 : Assumed Failure surface

Using a modified Coulomb criterion of sliding failure, they derived a direct relationship between pullout force P and compressive strength f'_c, for the geometrical dimensions of the Danish pullout system [Jensen and Bræstrup (1976)]. In 1994, Yener pointed out that the Jensen-Bræstrup directly proportional relationship between P and f'_c follows from the failure mechanism of concrete under pullout force to be assumed at the outset as a conic frustum [Yener (1994)]. He showed that once any mode of failure is assumed as the limiting state of behavior, the rigid body equilibrium on the corresponding free body diagram can be used to derive an expression relating$P$ and f'_c, without any reference to plasticity.

Nonlinear finite element analysis. In 1981, Ottosen published a nonlinear analysis on Lok-Test, using axisymmetric triangular elements (Fig. 4) with linear displacement functions. The progressive development of radial and circumferential cracks are illustrated in Fig. 5 [Ottosen (1981)]. The distribution of principal stresses at 70 percent loading indicated that large compressive forces run from the disk in a narrow band toward the reaction ring. Hence, the reserve pullout capacity was attributed to crushing of the concrete within this compression band. It is nevertheless reported [Stone and Carino (1983)] that there was no visible evidence in the tested specimens of a band of crushed concrete along the failure surface which would confirm compression failure.

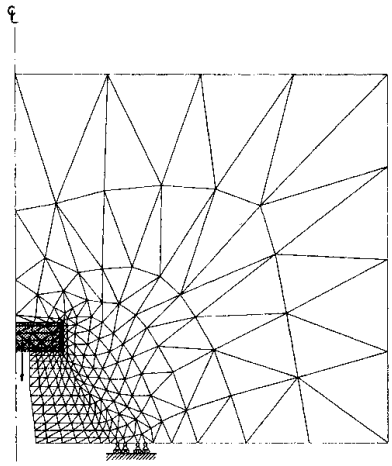

Figure 4 : Axisymmetric finite element mesh for Lok-Test

Moreover, Stone and Carino criticized the Ottosen bond between the pullout disk and the surrounding concrete, which was assumed to be perfect, since pullout inserts are generally oil-coated prior to installation [Stone and Carino (1983)].

Linear-elastic finite element analysis. In Stone and Carino (1984), a linear-elastic axisymmetric finite element analysis is reported for studying the stresses induced in concrete before cracking. It was seen that before cracking there are tensile stresses that are approximately perpendicular to the eventual failure surface, and that compressive stresses are directed from the insert head toward the ring (Fig. 6). These principal stresses are nonuniform and are greatest near the top edge of the insert head.

Stone and Carino suggested that the pullout strength is not governed directly by compressive strength, and that an alternative explanation needs to be found for the experimentally observed close correlation between these two strengths. The investigators concluded that failure is governed primarily by the tensile strength of mortar, and occurs when sufficient aggregate particles have been pulled out of the mortar matrix.

Using linear-elastic fracture mechanics together with a two-dimensional model, Ballarini, Shah and Keer (1986) have concluded that ultimate load is governed by the fracture toughness of the matrix.

Yener (1994) objected that an interpretation drawn from a linear-elastic analysis does not provide sufficient information on the concrete progressive failure, since concrete cracking initiates at a load which is only a small fraction of the failure load.

Nonlinear fracture mechanics analysis. The discrete cracking model by Hellier, Sansalone, Carino, Stone and Ingraffea (1987) shows excellent agreement between the predicted and observed internal cracking in the pullout test (Fig. 7). A primary circumferential crack develops at the corner of the insert head and propagates outward at a shallow angle. This crack ceases to grow when it penetrates a tensile-free region. A secondary crack develops subsequently, coinciding with the observed final fracture surface. This study also concluded that failure does not occur by uniaxial compressive failure in concrete.

Discrete cohesive crack model. An axisymmetric finite element model, based on linear strain 6-noded triangles, was used by Bocca, Carpinteri and Valente (1989). The fracture process was simulated by means of a nonlinear discrete cracking approach. The fictitious crack length is assumed as the driving parameter in the numerical simulation. The crack propagates normally to the maximum tensile stress. Outside of the crack the material is linear elastic and isotropic. The interface between the upper side of the steel disc and the concrete is assumed to be adhesive. All other interfaces between steel rod and concrete are considered as non-adhesive. Therefore, the disc only has been modeled and the pullout force has been applied directly to the steel disc. A modification of the mesh is required at each step of the crack propagation process. The mesh used at step 24 is reported in Fig. 8.

An experimental programme has been performed in Bocca, Carpinteri and Valente (1989) in order to compare

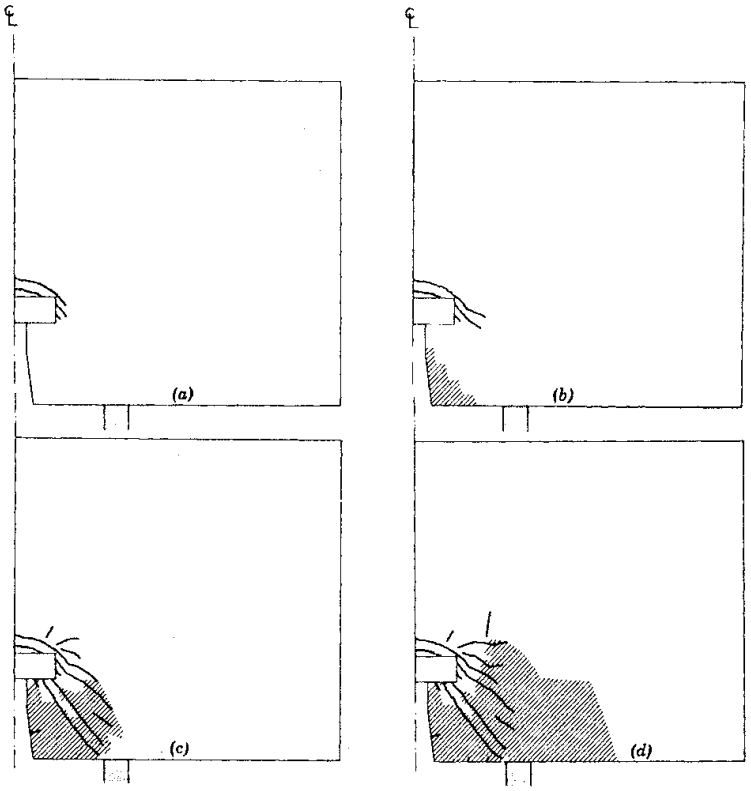

Figure 5 : Crack development with increasing loading, in relation to predicted failure load (a) loading = 15%; (b) loading = 25%; (c) loading = 64%; (d) loading = 98%

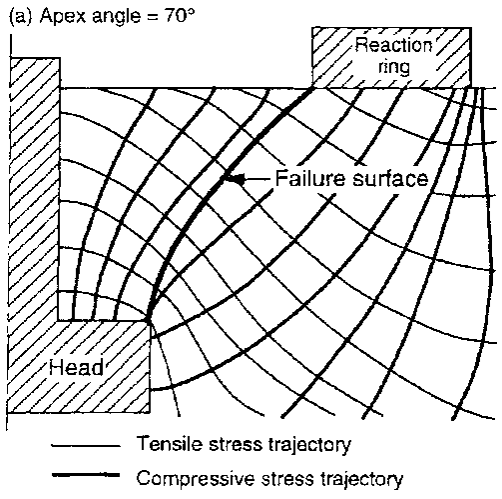

Figure 6 : Principal stress trajectory prior to cracking in homogeneous materials

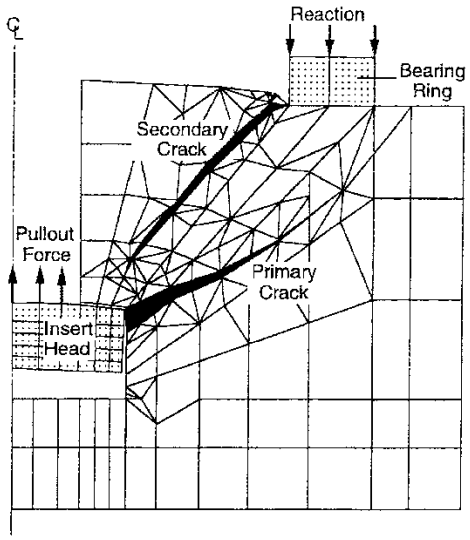

Figure 7 : Predicted circumferential cracks

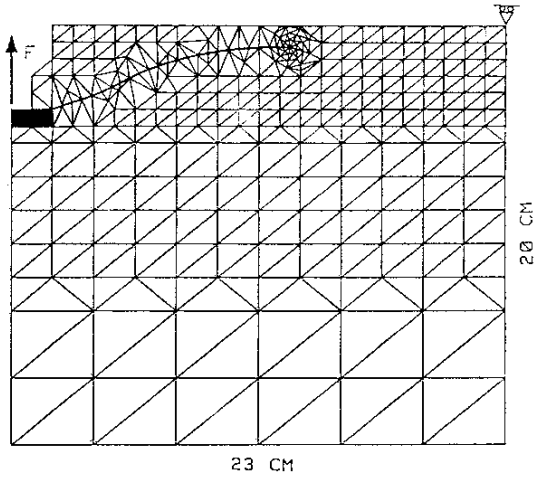

Figure 8 : Finite element mesh at step 24

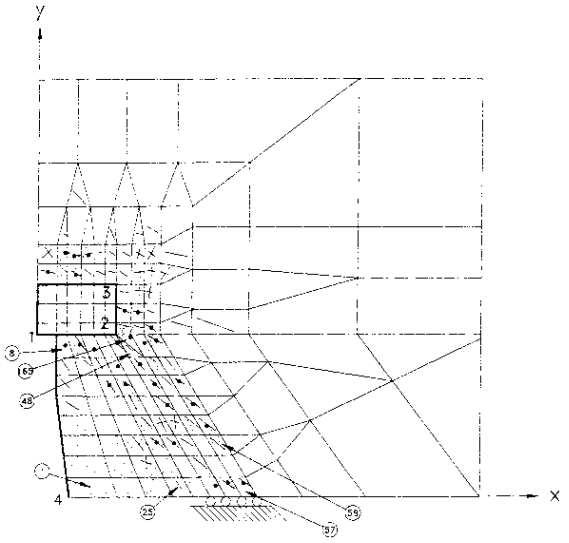

Figure 9 : Finite element mesh and predicted failure

results. The pullout tests were carried out by varying the internal diameter ϕ of the contrast ring, whereas the rod depth h and the rod head diameter d were maintained unchanged. The apex angle (2α in Fig. 1) was varied from 41° to 143°. A good theoretical-experimental correlation was found in force versus displacement diagrams, for the case of large contrast ring.

The performed experimental tests for large contrast ring show that the crack formation is influenced only by the material properties and not by the contrast diameter. The failure process is dominated by tensile cracking and the failure surface follows the aggregate contours, so that the aggregate remains unbroken. By decreasing the apex angle, the failure mechanism changes and the failure surface is increasingly influenced by the contrast ring. For small contrast ring, the failure mechanism is complex, as the mortar versus aggregate interaction and interlock prevail. The aggregate shearing is accompanied by a capillary mortar crushing.

Plastic-fracture finite element analysis. This analysis was performed by Yener, in 1994. The assumptions used in post-fracture analysis are: the crack direction is normal to the direction of the maximum principal strain; the fracture mode consists of cracking and crushing; the post-fracture constitutive relationship is anisotropic elastic. Moreover, the pure crushing zone has no strength and the pure cracking zone has no strength in the cracked plane when the crack is open. The post-fracture model permits shear transfer through the cracked plane by means of aggregate interlock. The strain softening of the material is not considered. The modified von Mises and dual-function material constitutive models were used in combination with the five-parameter failure criterion, and linear quadrilateral finite elements were employed. The axisymmetric finite element mesh is shown in Fig. 9. The behavior of concrete is described by referring to the scheme in Fig. 10.

Failure is said to occur by outward crushing of concrete around the perimeter of the failure cone near the reaction ring. In agreement with experimental results, depending upon the values of h, d, and d_1 (Fig. 3), the failure surface of the extracted concrete may resemble a trumpet shape, rather than a conic frustum. Moreover, it was found that the behavior of concrete is primarily controlled by combined compression and bending actions. The bending action becomes pronounced during the latter stages of loading.

While the conclusions of the reported studies differed, it is generally agreed that circumferential cracking (producing the failure cone) begins at highly stressed regions next to the insert head at a pullout load that is a fraction of the ultimate value. With increasing load, the circumferential cracking propagates toward the reaction ring. However, there is no agreement on the nature of the final failure mechanism governing the magnitude of the ultimate pullout load.

The failure mechanism was further investigated experimentally by Krenchel [Krenchel (1985)]. He loaded sam-

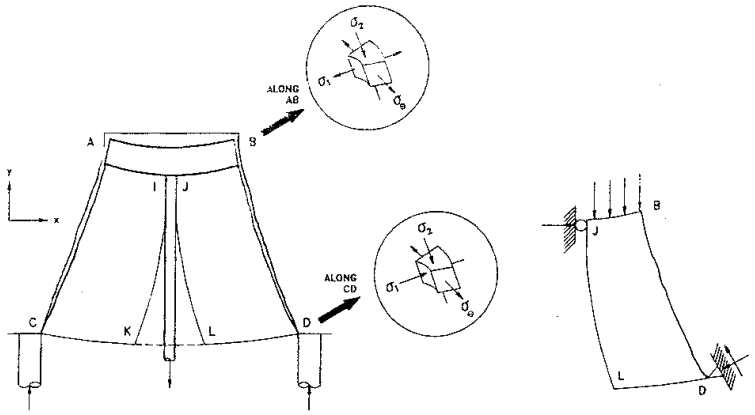

Figure 10 : Complete failure surface (a) stresses and deformations; (b) load-carrying mechanism

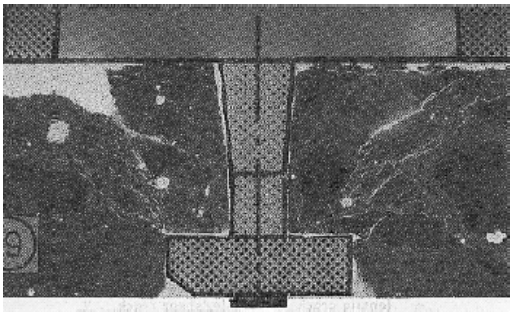

Figure 11 : Crack analysis after de-loading

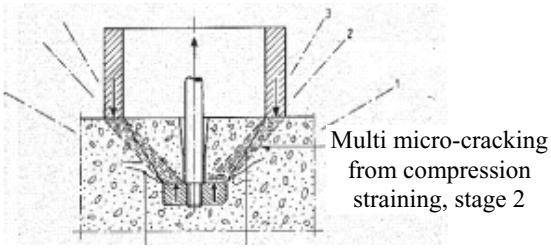

Figure 12 : The three different stages of internal cracking

ples to different levels on the load-displacement curve. Afterwards, the samples were saw-cut through their axis, the surfaces were ground smooth and impregnated with epoxy containing a fluorescent dye to reveal cracks under ultraviolet light (Fig. 11). It was found that the internal rupture is a multistage process where three different stages, each with different fracture mechanism, can be clearly separated (Fig. 12). In the first stage, tensile cracks begin, starting from the notch formed by the upper edge of the pullout disc. In the second stage, a multitude of stable microcracks are formed in the above mentioned truncated zone. Even after the load has stabilized at the peak point, the third stage occurs. This forms a tensile-shear crack running all the way around from the outside edge of the disc to the inside edge of the counterpressure ring.

3 General remarks on the remeshing CM code

The theoretical basics of the Cell Method (CM) have been developed by Tonti [Tonti (2001)]. The essence of the CM is to provide a direct finite formulation of field equations, without requiring a differential formulation, such as shown in Fig. 13.

The main differences between variational and discrete formulation are summarized in Fig. 14. In particular, it will be showed here how heterogeneities do not represent an obstacle with the CM, and how it is possible to easily treat domains with several materials.

The CM uses two meshes, the one the dual of the other. Here, a Delaunay/Voronoi mesh generator [George (1995)] is used to generate the two meshes in two-dimensional domains (Fig. 15).

In crack propagation problems, the geometry of the mesh must be modified as the crack propagates. The ability of the CM code with remeshing to take a general change in the mesh topology easily into account has been shown

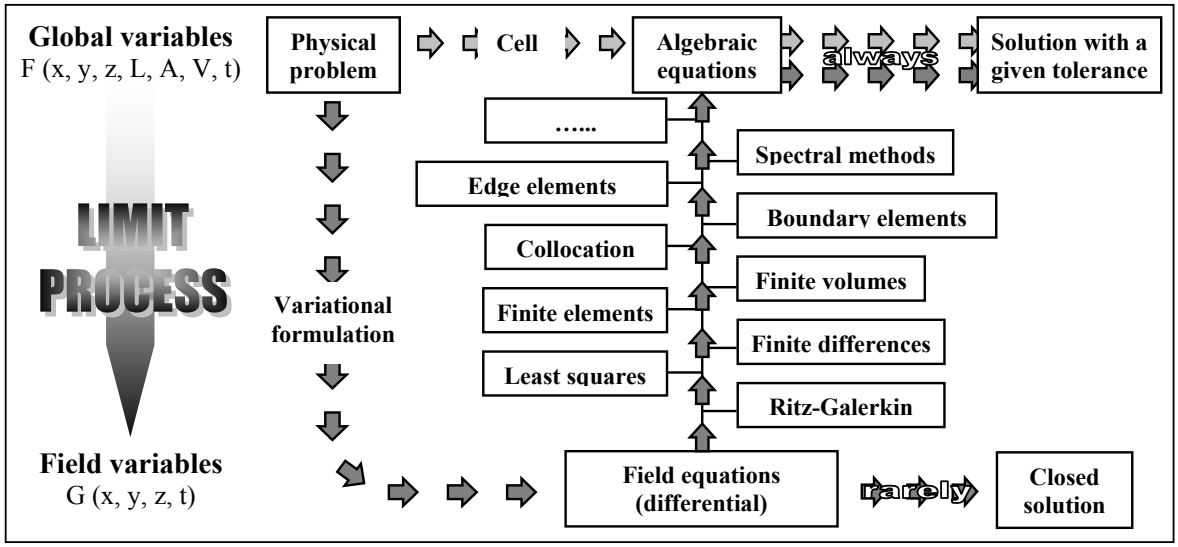

Figure 13 : Way to achieve the solution thought the Cell and Variational formulation

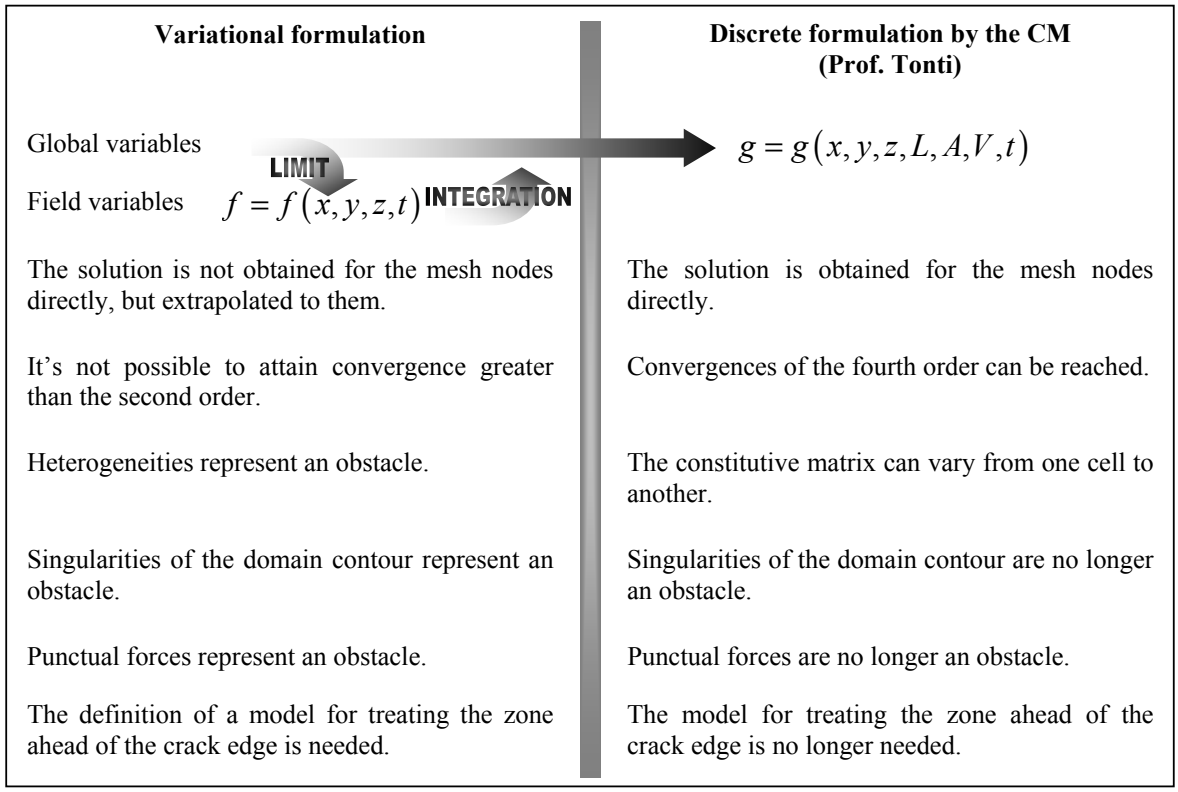

Figure 14 : Main differences between the variational and the discrete formulation by the CM

in Ferretti (2003). This ability is all the more relevant since changes in mesh topology are rarely supported by classical finite element method (FEM) numerical codes.

Of the two strategies available for studying fracture mechanics (FM) using the FEM (Fig. 16), the one describing the crack as a displacement discontinuity has been chosen in the CM code with remeshing. For model-

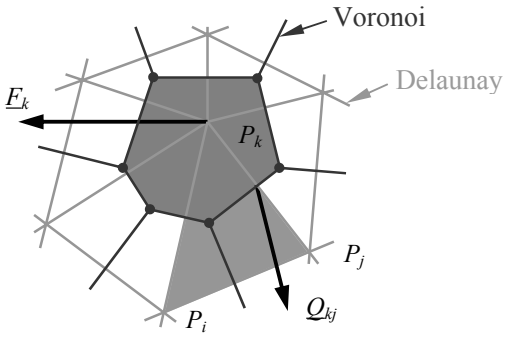

Figure 15 : Mesh of Delaunay/Voronoi

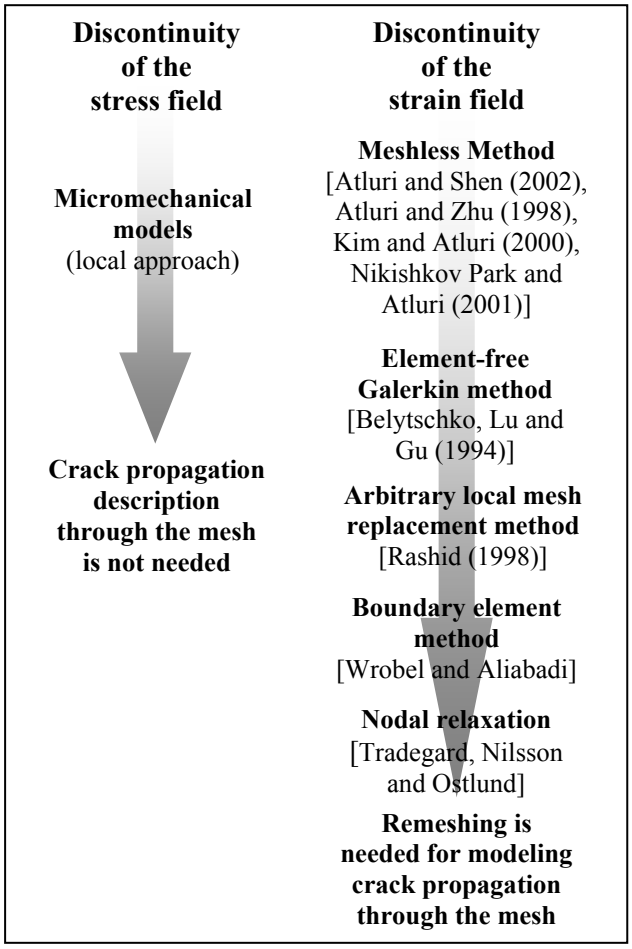

Figure 16 : Stratagies available to study fracture mechanics using FEM; sharp drop in normal stress and displacement discontinuity

ing the crack propagation through the mesh, as required by this strategy, the nodal relaxation technique has been

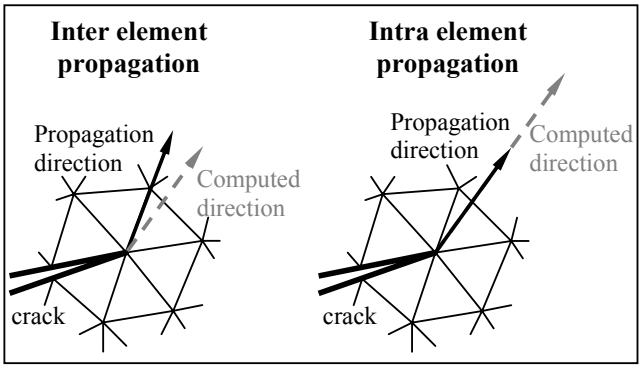

Figure 17 : Inter and intra element propagation for the nodal relaxation technique

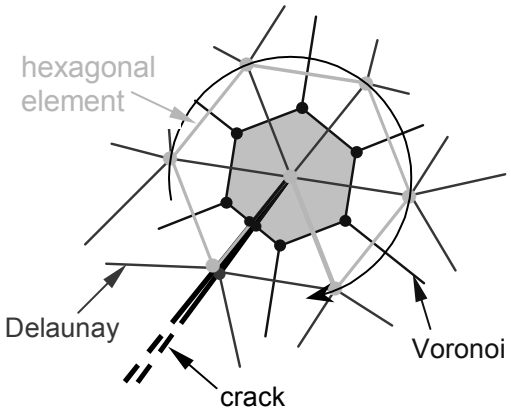

Figure 18 : Special element for stress analysis

adopted. This technique can be achieved using inter-element propagation or intra-element propagation (Fig. 17). Inter-element propagation is mesh dependent, since the crack propagates along the mesh side nearest to the computed propagation direction. On the contrary, intra-element propagation is mesh independent, since the crack propagates along the computed propagation direction. This takes more computational time for regenerating the mesh, but leads to more accurate results. The code here employed uses the nodal relaxation with intra-element propagation technique.

Finally, a special hexagonal element has been inserted at the crack tip (Fig. 18), for regularizing the shape of the mesh surrounding the tip. Since the CM associates geometrical objects of the dual mesh to source variables, this regularization allows description of the stress field in a finite neighborhood of the tip [Ferretti (2003)]. In the

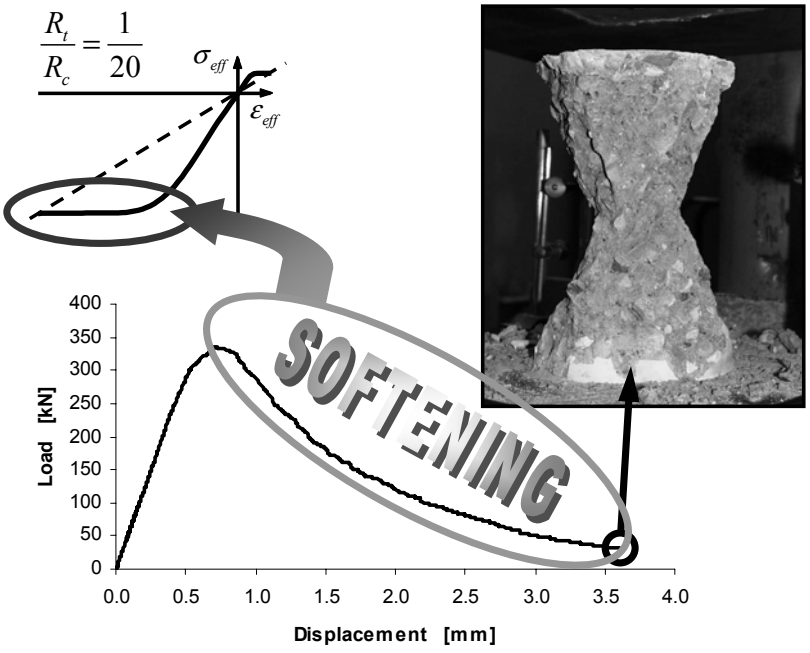

Figure 19 : Numerical load-displacement diagram for plain concrete specimens

remainder of the domain, the mesh generator is allowed to generate the mesh automatically.

Further details on the remeshing CM code are collected in Ferretti (2003).

4 Constitutive assumptions

The concrete constitutive law adopted in this study is monotonically non-decreasing (Fig. 19), in accordance with the identification procedure for concrete in monoaxial load provided by Ferretti (2001). The main effort of this procedure is to separate the actual material behavior from the structural behavior, always affecting experimental data. This results in a constitutive law characterizing the behavior of the material in the specimen internal core, the resistant structure carrying load even at the very end of the compressive test (Fig. 19). The idea underlying this procedure is that strain-softening is not a material property, but is essentially due to scaling the applied force by the original cross-sectional area rather than the actual cross-sectional area. Through microseismic measurements and energetic considerations, the procedure identifies the actual cross-sectional area, leading to a material monotone behavior.

From the beginning of the 20th century forth, a number of researchers have questioned whether strain-softening is a real material property or merely the result of inhomogeneous deformation caused by the experimental technique [Hadamard (1903); Bishop and Green (1965); Kirkpatrick and Belshaw (1968); Hudson Brown and Fairhurst (1971); Deman (1975); Hettler (1981); Dresher A. and Vardoulakis (1982); Bergan (1983); Hegemier and Read (1983); Sandler and Wright (1983); Wu and Freud (1983)].

They produced a series of studies, all sharing the common idea of non constitutive nature of the softening behaviour. Nevertheless, they were not able to provide an identifying procedure from the experimental data to a monotone constitutive law for concrete. They only treated the problem under the theoretical point of view, since it was estimated [Hegemier and Read (1983)] to be extremely difficult, if not impossible, to experimentally track the effective cross-sectional area at each stage of the failure process. The impossibility to achieve a new constitutive proposal is the main reason why this field of research fell rapidly out of favour. In Ferretti (2001), theoretical considerations on the non-constitutive nature of strain-softening were supported by a new identification proposal for material properties, and this led to a revival of the research field.

It was shown [Ferretti (2001), Ferretti and Bastianini (2002)] how the monotone law identified by Ferretti

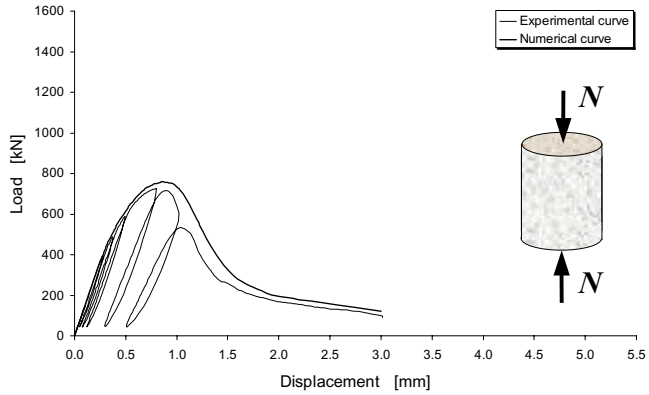

Figure 20 : Numerical load-displacement diagram for plain concrete specimens

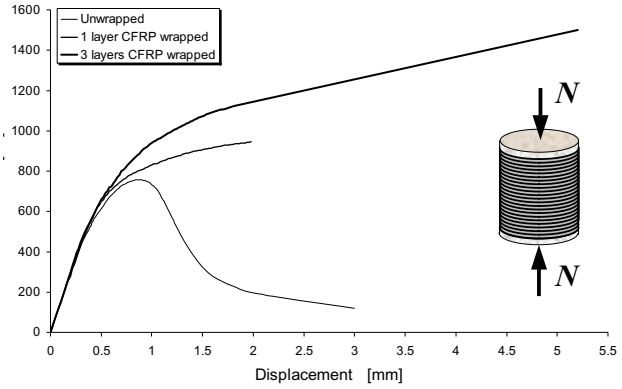

Figure 21 : Numerical load-displacement diagram for wrapped and unwrapped and concrete specimens

(2001) turns out to be size and failure mechanism insensitive for mono-axial compressive load. This result made it possible to formulate a new concrete law in mono-axial compressive loading, the effective law, which can be considered to be more representative of the material physical properties than the softening laws are.

The effective law was used as input datum in the remeshing CM code for modeling the compressive tests on six specimens with varying slenderness [Ferretti (2001)].

In agreement with the experimental results, the numerical load-displacement diagrams turns out to be softening (Fig. 20). Moreover, the size-effect on the six geometries is well reproduced. As concerns the numerical crack path, it is very close to the experimental crack path, for each geometry.

The extension of the effective law to the triaxial compressive field [Ferretti (2001); Ferretti and Di Leo (2003)] made it possible to model compressive tests on wrapped concrete cylinders. In Fig. 21, the numerical load-displacement diagrams for cylinders wrapped with carbon fiber sheets are provided.

Finally, the extension of the effective law to the tensile field was made on the assumption that the ratio between tensile and compressive strength, R_t and R_c, is equal to $1/20$ (Fig. 19). This made it possible to test the effective law for applications in bi-axial tensile load [Ferretti Viola and Di Leo (2002-a); Ferretti Viola and Di Leo (2002-b)]. The stress field analysis provided by the remeshing CM code for a cracked plate in bi-axial tension is plotted in Fig. 22.

5 Numerical results

Numerical results concerning the pullout test modeling through the remeshing CM code will be presented here.

Since the dimensions of the concrete specimen are very large in comparison to the dimensions of the steel insert, they can be assumed to be infinite. Because of axial symmetry (Fig. 23), only one half of the domain has been modeled. Although physically the problem is three-dimensional, the axisymmetry allows mathematical treatment of the problem in two-dimensions.

One analysis on the extinction zone of the load transferred by the steel insert has been performed (Fig. 23), in order to identify the minimum finite geometry correctly reproducing the stress-strain field around the steel insert. For simplicity, the minimum finite geometry has been assumed to be square shaped (Fig. 23). This geometry has then been used as modeling domain in the CM remeshing code.

5.1 Identification of the unknown boundary conditions

The pullout test is a typical example of crack propagation in Mixed Mode loading, since the load is applied obliquely both to the crack propagation direction and to the crack opening direction. For such a type of load, the combination of loading and boundary conditions forces the edges of the crack to close at some point. At those points, Mode II loading prevails. At the remaining points, the two edges of the crack separate and Mode

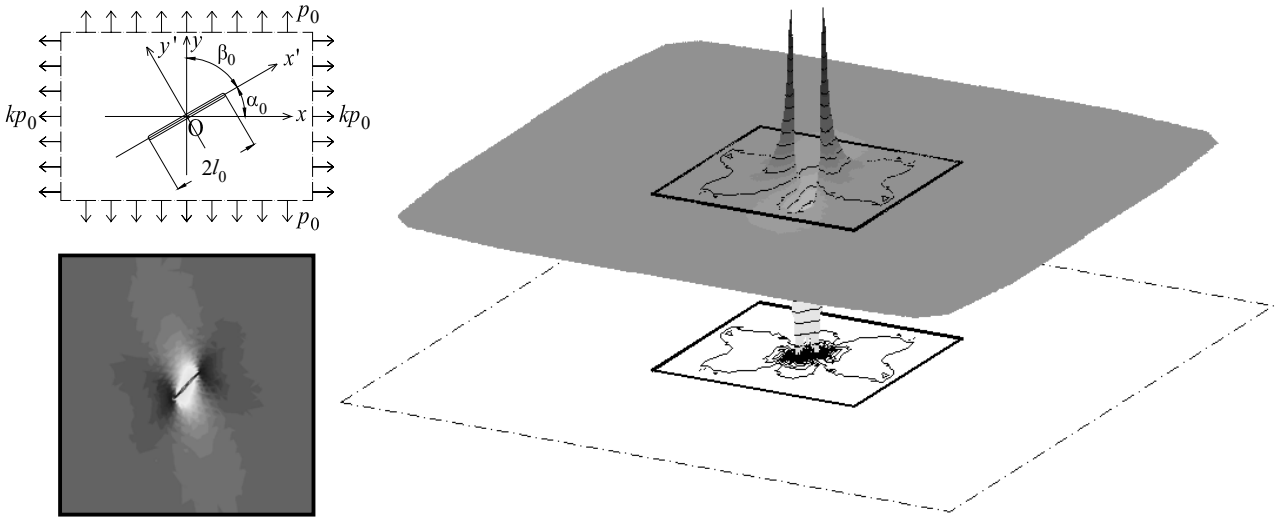

Figure 22 : 2D and 3D stress field analysis for a cracked plate in bi-axial loading

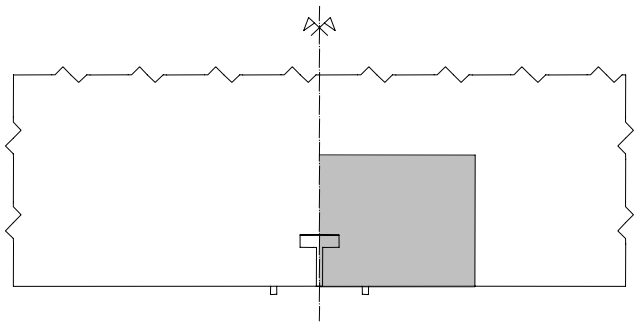

Figure 23 : Geometry to model and stress extinction zone of the load transferred by the steel insert

I loading prevails. Points separating the zones in which Mode I loading prevails from those in which Mode II loading prevails are a function of the load step and crack length. They thus represent an unknown of the Mixed-Mode problem and must be identified before the numerical stress analysis takes place.

Not only the crack edges are subjected to Mixed-Mode loading in the pullout test. There are indeed other surfaces which can separate or slide over each other, developing constraint reactions. They are the surfaces separating the steel insert from the concrete specimen. In this second case, the surfaces cannot evolve, but the point separating the Mode I loading zone from the Mode II loading zone is still an unknown of the Mixed-Mode loading problem.

As has been shown in Ferretti (2003), the CM remeshing code is automatically able to estimate which part of the boundary is subjected to Mode I loading, and which part is subjected to Mode II loading. A friction model has been used there to assess the forces acting across the crack surfaces. The code presented in Ferretti (2003) represents the first case for which a sliding contact problem is solved by means of the CM. It can be considered as the equivalent in the discrete formulation of the FEM contact elements for the variational formulation [Har (1998), Papadopoulos, Jones and Solberg (1995), Zhong (1993)]. The result of the boundary condition identification on the surfaces separating the steel insert from the concrete specimen is shown in Figs. 24÷26 for the geometry of the Lok-Test.

5.2 Analysis of the stress field

As shown in Fig. 23, the geometrical domain to be modeled can be considered as semi-infinite. The impossibility for a numerical code to operate on a semi-infinite geometry, obliges us to reduce the analysis to a geometry of finite dimensions. This finite geometry is delimited by the symmetry axis, the external boundaries of the steel insert and concrete specimen, and an internal concrete boundary, consisting of one horizontal and one vertical side of equal dimensions (Fig. 23). The boundary conditions on the symmetry axis are represented by horizontal double pendulum constraints (constrained horizontal displacements and free vertical displacements). Horizontal

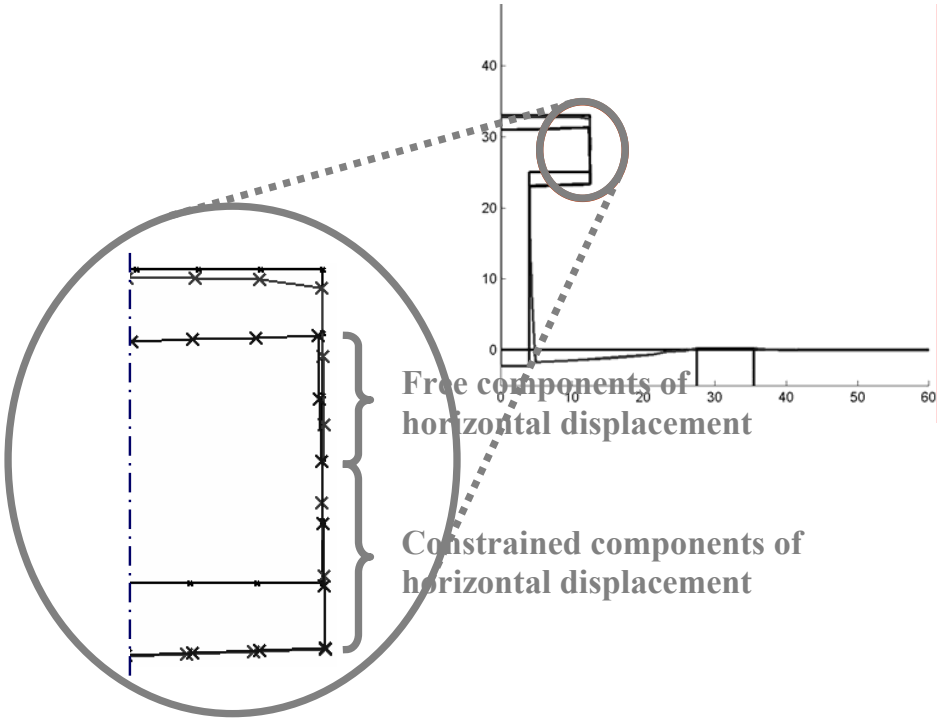

Figure 24 : Deformed configuration and detail of the identified boundary conditions on the disk thickness

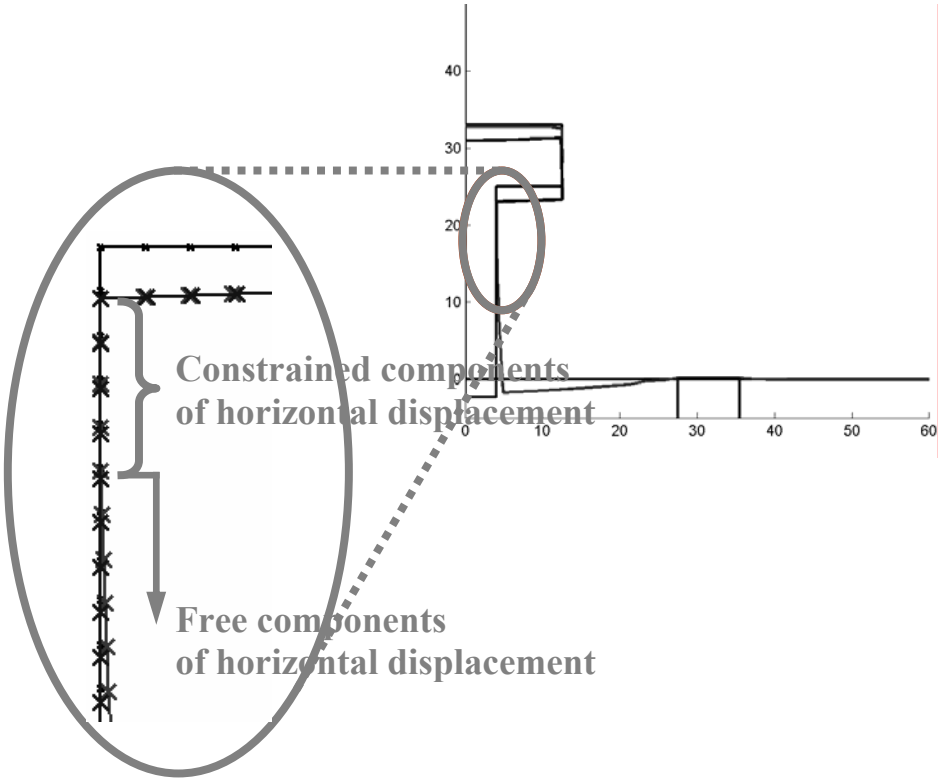

Figure 25 : Deformed configuration and detail of the identified boundary conditions on the rod

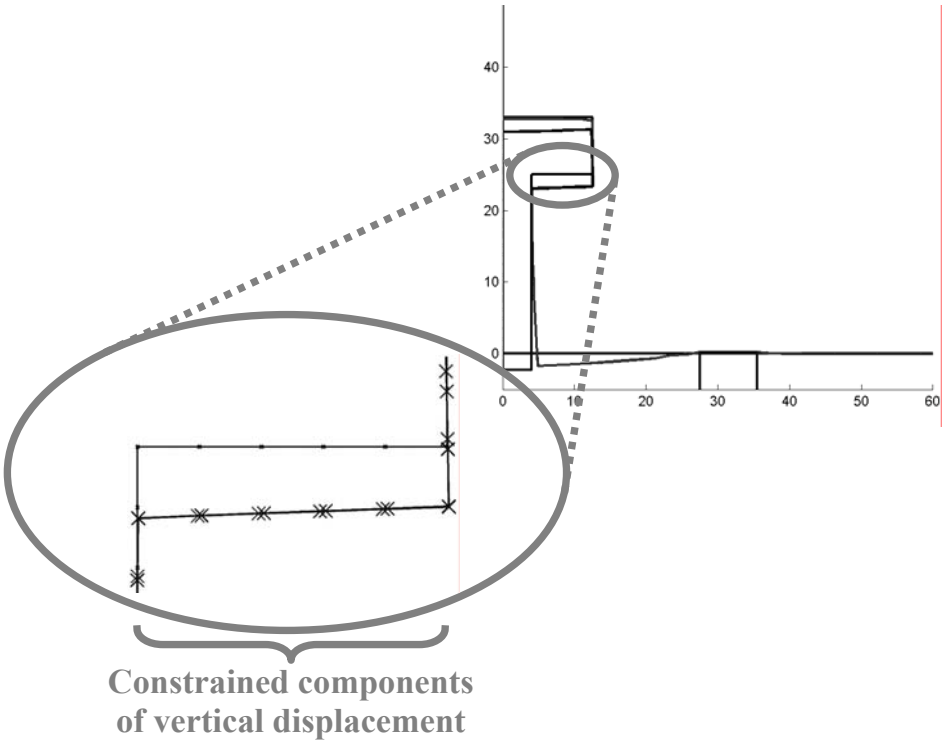

Figure 26 : Deformed configuration and detail of the identified boundary conditions on the disk lower edge

and vertical displacements on the external boundary are constrained for the nodes lying on the counterpressure ring and are free elsewhere. The simulation has been performed in displacement-control, by imposing the relative displacement between the rod lower edge and the counterpressure ring upper edge. The counterpressure ring has been assumed to be perfectly rigid. It has been considered as an external constraint, and it does not belong to the modeled domain. The zero value of absolute vertical displacements on the external boundary has been fixed on the lower right corner of the extinction zone (assumption of zero displacement at infinity). For this choice of absolute displacement, it was possible to estimate the punching effect on the concrete-counterpressure ring interface (Fig. 27).

Figure 27 : Deformed and undeformed configuration near the counterpresuure ring

Boundary conditions on the internal boundary are functions of the internal boundary dimensions. These were identified as those dimensions for which the stresses on the internal boundary approach zero value (within a certain tolerance). That is to say, the internal boundary has been placed on the contour of the stress extinction zone.

Finally, the bond between the pullout disk and the concrete above the disk has been assumed to be monolateral, with the steel nodes free to move downward with regard to the concrete nodes, from the beginning of the test forth.

A number of graphical tools were developed together with the CM remeshing code [Ferretti (2001)], in order to draw the stress-strain field in the modeled domain. The graphical tool for the principal directions drawing provides each Delaunay element with a segment centered on the element circumcenter, whose direction is that of the principal direction, and whose length is scaled by the principal stress (Fig. 28). Principal directions and principal values are computed in the element circumcenter. From Fig. 28, one can appreciate how the principal

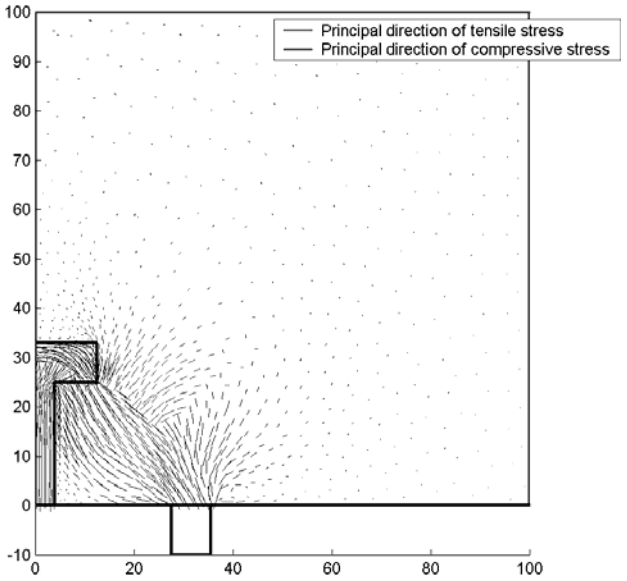

Figure 28 : Numerical principal and principal stresses for the geometry of the Lok-test

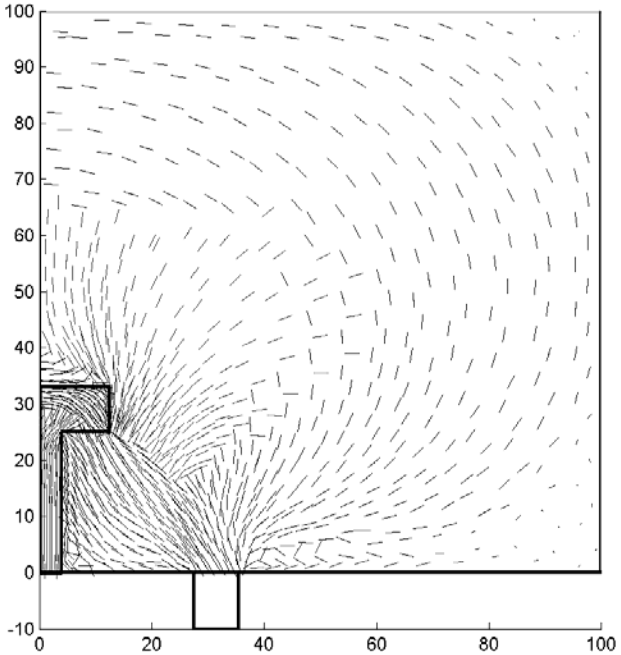

Figure 29 : Tangent to the principal trajectories for the geometry of the Lok-test

stresses approach zero value on the internal boundary, for the chosen dimensions of the modeling domain in the Lok-test case. The behavior of the principal directions before cracking can be appreciated in Fig. 29, obtained from Fig. 28 by providing each element loaded above a certain value of stress with a segment of fixed length. These directions are tangent to tensile and compressive stress trajectories, quite similar to those provided by the linear-elastic finite element analysis of Stone and Carino (Fig. 6, [Stone and Carino (1984)]).

The CM analysis of the stress field between the steel insert and the counterpressure ring (Fig. 28) exhibits very large a stress transferring zone of compressive forces.

As will be discussed in the following, the stress transferring zone grows thin as the crack propagates from the disk toward the counterpressure ring. Approaching the ultimate load, a narrow compressed band of stress transferring can be identified, as in the analysis of Ottosen [Ottosen (1981)]. The large portion of specimen interested by the stress transferring mechanism before cracking is also given by the graphic tool for the stress discrete drawing in the axial direction (Fig. 30). Fig. 30 also shows the pouncing effect on the stress field at the disk-specimen and counterpressure ring-specimen interfaces.

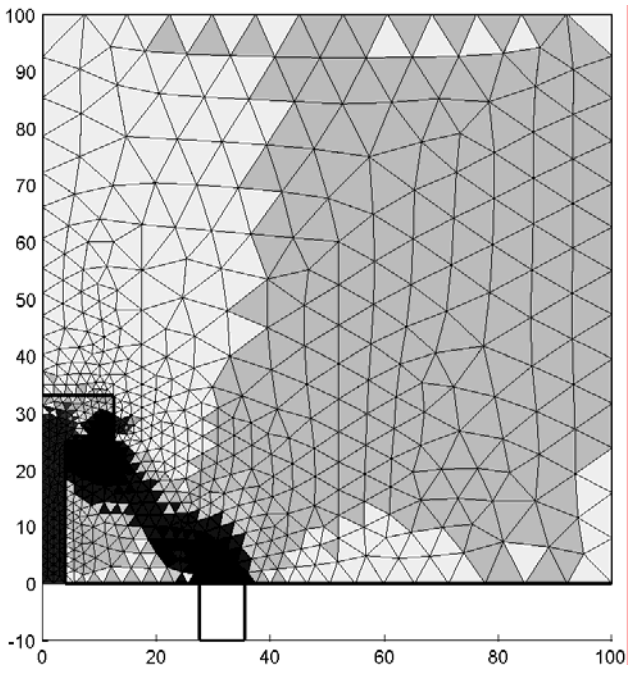

Figure 30 : Discrete stress analysis for the geometry of the Lok-test

The analysis of the stress field is completed by the tool

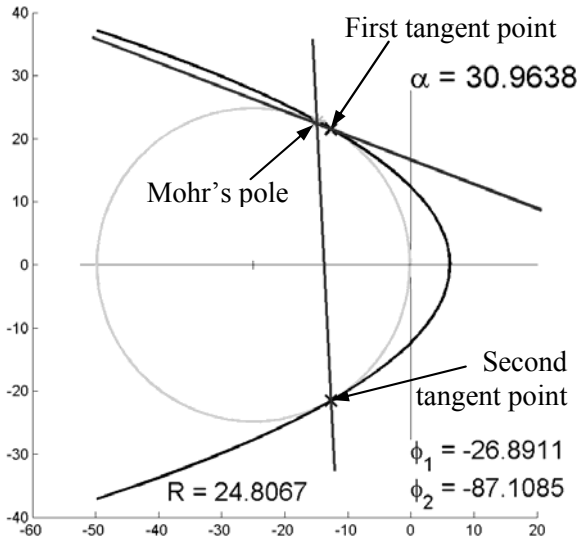

Figure 31 : Limit condition and directions of first propagation for geometry of the Lok-test

for computing the crack propagation direction proposed in Ferretti (2003). The analysis in the Mohr-Coulomb plane and the crack geometry updating before remeshing activation are the same as in Ferretti (2003). The difference between the present numerical simulation and the one presented in Ferretti (2003) concerns the failure criterion, since, this second time, the Leon criterion was used:

$$\tau_n^2 = \frac{c}{f_c}\left(\frac{f_{tb}}{f_c} + \sigma_n\right). \tag{1}$$

In Eq. 1, c is the cohesion, f_c the compressive strength, and f_{tb} the tensile strength.

The choice of the Leon criterion is due to the mechanism of failure activation, which can manifest themselves both in the compressive and tensile field. The Mohr-Coulomb criterion used in Ferretti (2003) is sufficiently adequate to describe the propagation direction for failure mechanism in the compressive field, while it is not adequate in the case of failure mechanisms in the tensile field. On the contrary, the Leon criterion is quite adequate for describing the direction of propagation both in the compressive and in the tensile field.

The two directions of first propagation for the Lok-test geometry are shown in Fig. 31. They are given by the directions of the lines that join the Mohr's pole to the two tangent points. When the limit condition is reached, both the directions activate, and two cracks then enucleate. The direction with the minimum slope (in magnitude) with regard to the σ axis was denoted as first direction of propagation, and the direction with the maximum slope (in magnitude) with regard to the σ axis was denoted as second direction of propagation (Fig. 31). Since experimental results show that the crack along the first direction of propagation stops soon after its initiation [Krenchel (1985)], only the second direction of propagation has been considered in the numerical simulation. The crack paths presented in the following are then relative to the second direction of propagation.

5.3 Analysis of the mechanism of crack initiation

Experimental results show that the crack initiation mechanism in the pullout test depends on the geometry of the pullout apparatus [Bocca, Carpinteri and Valente (1989)]. In particular, the ratio between the internal diameter of the counterpressure ring and the rod depth is decisive in establishing the type of failure process. That is, the failure mechanism depends on the angle α, defined as in Fig. 1. Nevertheless, experimental results are not exhaustive in describing the dependence of the initiation mechanism from α. This leads to the impossibility of identifying a unified model, able to correctly describe the failure mechanism for varying values of α. Such a type of model is of fundamental importance when a numerical analysis based on the equilibrium of the concrete to be extracted is attempted [Jensen and Bræstrup (1976)]. In this work, the CM remeshing code is proposed as an analysis instrument for identifying the correlation between initiation mechanism and α. This is possible since the CM remeshing code operates on both the steel and concrete domains, automatically computing the boundary conditions on the steel-concrete interface. The definition of a steel-concrete behavior model is not needed and the simplified numerical analysis of equilibrium on the concrete to be extracted is not required. No a-priori assumptions have then been done on the steel-concrete interaction. This last has been identified a-posteriori, as an output of the numerical simulation.

The angle α (Fig. 1) has been chosen as the geometrical parameter of the steel-concrete interaction. In the following, all values of α will be provided in degrees.

The analysis of the initiation mechanism has been performed in the Mohr-Coulomb plane, such as in Ferretti (2003). The failure criterion adopted is the Leon crite-

rion. For this criterion, the limit surface in the Mohr-Coulomb plane is parabolic (Fig. 31).

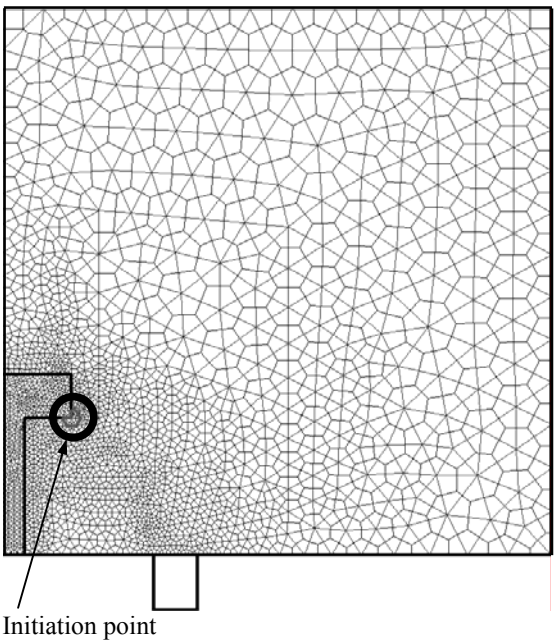

Figure 32 : Meshed domain and initiation point

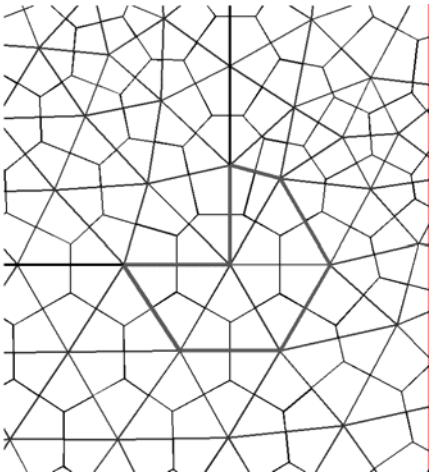

Figure 33 : Special element for stress analysis on the domain contour (detail of fig 32)

The initiation point has been fixed on the right-bottom corner of the disk (Fig. 32), in agreement with experimental [Krenchel (1985)] and previous numerical results [Ottosen (1981); Stone and Carino (1984); Hellier, Sansalone, Carino and Ingraffea (1987); Bocca, Carpinteri and Valente (1989); Yener (1994)]. On this point, the special element for stress analysis has been inserted (Fig. 32). The special element used here is a refinement of the special hexagonal element used in Ferretti (2003) (Fig. 18), which was studied to be inserted at the crack tip of pre-cracked specimens. Pre-cracking specimens is very common in numerical simulations, since it is difficult to determine where the crack will start. Micro-failures and inclusions always induce local stress concentrations, from which failures and cracks originate. These defects cannot realistically be taken into account numerically in large-scale models.

Consequently, one must either assume the material to be perfect or impose the point of crack initiation by pre-cracking the specimen. In Ferretti (2003) specimens were pre-cracked, assuming a crack initiation direction in accordance with the experimental direction of first propagation. Here, the direction of first propagation is an unknown of the problem, since it is one of the quantities affected by the dependence from α. Consequently, pre-cracking was not possible in the pullout test modeling.

The special element for stress analysis was then inserted on the known point of initiation, which is a point of the steel-concrete interface. To prevent the special element from intersecting the steel-concrete interface, the geometry of the special element for the first propagation step has been modified as shown in Fig. 33. For further propagation steps, the same hexagonal element as the one used in Ferretti (2003) has been inserted at the crack tip.

The special element positioning tool for the first and the further propagation steps operates as follows:-

- The input file for the mesh generator, which defines the geometry of the domain, is modified to add four (six) new nodes, equidistant from the element insertion point;
- The desired element dimension [Ferretti (2003)] for the four (six) new nodes and for the tip node is set equal to the distance between the new nodes and the element insertion point;
- The input file for the mesh generator is modified to add seven new sides which join the new nodes and the insertion point in a counter-clockwise sense, without crossing the surface of the crack;

- A marker is associated with the seven new sides, indicating that the polygon that starts and ends with the insertion point, and touches all the new points, is a false hole [Ferretti (2003)].
- As in Ferretti (2003), the mesh generator treats the boundary chain of a false hole as a closed internal interface between two parts of the domain. This leads to specifying a particular mesh geometry in the neighborhood of the element insertion point, with four (five) equilateral triangles. The Voronoi mesh which follows from the special element insertion presents a semi-regular (regular) Voronoi polygon centered on the element insertion point. The association between the sides of this Voronoi cell which are equidistant from the element insertion point and the stress field around the element insertion point itself is shown in Ferretti (2003).

The load of crack initiation has been computed from the step-wise identification of the (relative) displacement of crack initiation (simulation in displacement-control):-

- A displacement of first approximation is considered, and the Mohr's circle of first approximation is identified for the neighborhood of the initiation point.
- If the Mohr's circle of first approximation intersects the limit surface, the displacement of first approximation is greater than the displacement of crack initiation. Thus, the displacement is halved, giving the displacement of second approximation.
- If the Mohr's circle of first approximation is internal to the limit surface, the displacement of first approximation is smaller than the displacement of crack initiation. Thus, the displacement is doubled, giving the displacement of second approximation.
- Step two and step three establish upper and lower bounds on the displacement of crack initiation. Interval halving is used to determine the actual displacement of crack initiation, for which the upper and lower bounds are equal (to within a particular tolerance).

Once the load of crack initiation has been identified, the intersection points between the corresponding Mohr's circle and the limit surface give the mechanism of failure initiation. Figs. 34÷38 provide the Mohr's circle at the limit condition for five values of the angle α. In Fig. 34, the two intersection points lie in the negative semi-plane of the normal stress. Both the corresponding values of shear and normal stresses are not negligible. One can then conclude that the value of the angle α equal to 26.5651° corresponds to a mechanism of failure initiation for shear-compression.

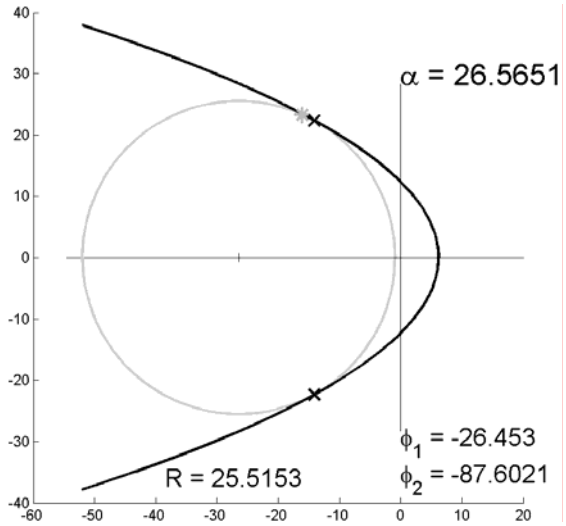

Figure 34 : Mohr limit analysis for a = 26.5651

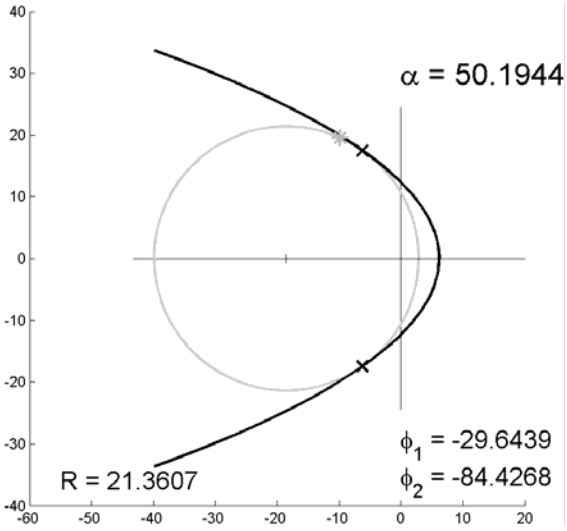

Figure 35 : Mohr limit analysis for a = 50.1944

An inspection of Fig. 31 clearly shows that also for the geometry of the Lok-Test ($\alpha = 30.9638^\circ$) the mechanism

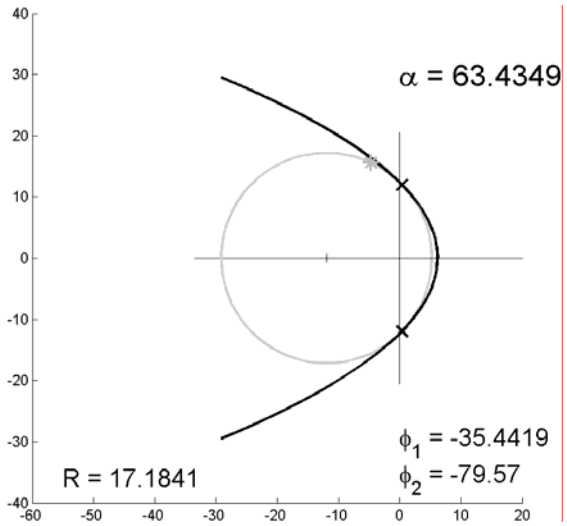

Figure 36 : Mohr limit analysis for a = 63.4349

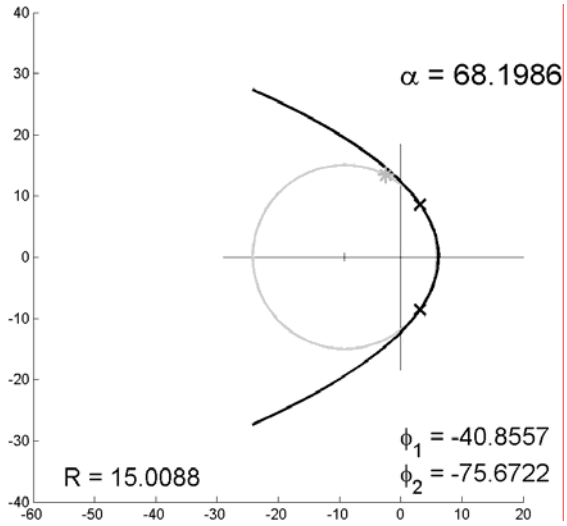

Figure 37 : Mohr limit analysis for a = 68.1986

of failure initiation is that of shear-compression.

Analogously, one can conclude that the values of the angle α equal to 50.1944°, 63.4349°, 68.1986° and 71.5651° correspond, respectively, to a mechanism of failure initiation for shear-compression (Fig. 35), pure shear (Fig. 36), shear-traction (Fig. 37), and pure traction (Fig. 38). This failure mechanism variability with α is in good accordance with the findings of the experimental programme of Bocca, Carpinteri and Valente (1989).

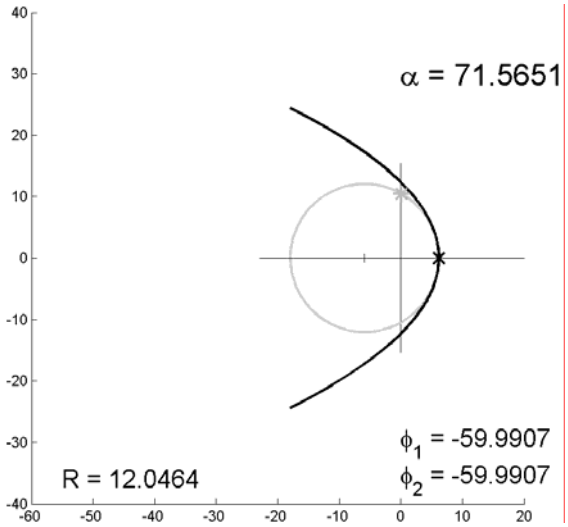

Figure 38 : Mohr limit analysis for a = 71.5651

5.4 Values of first propagation for varying diameter of the counterpressure ring

The numerically computed values of the radius of the Mohr's circle, the directions of first propagation, the load of first propagation, and the displacement of first propagation are given in Figs. 39÷42 for the angle α varying from the lower limit required by ASTM C 900 ($27° \leq \alpha \leq 35°$) and a value close to the upper limit of the experimental programme of Bocca, Carpinteri and Valente (1989) ($20.5° \leq \alpha \leq 71.5°$). The filled in regions in Figs. 39÷42 correspond to the ASTM C 900 requirements for α. As can be appreciated, the radius of the Mohr's circle, the first angle of first propagation, and the load of first propagation are decreasing with the angle α. The second angle of first propagation, lower than the first angle of first propagation, is increasing with the angle α, and equals the first angle of first propagation from the value of α corresponding to the mechanism of pure traction on ($\alpha \cong 71°$). Actually, when the failure mechanism is of pure traction the two intersection points and, then, the two propagation direction, coincide (Fig. 38). Finally, the displacement of first propagation is decreasing in the ASTM C 900 range of α. Then, it reaches a minimum for a value of α of about 38°. For greater values of α, the displacement of first propagation increases, reaching a maximum in correspondence of the pure shear failure mechanism ($\alpha \cong 63°$). From this point on, the behavior is decreasing with the angle α again.

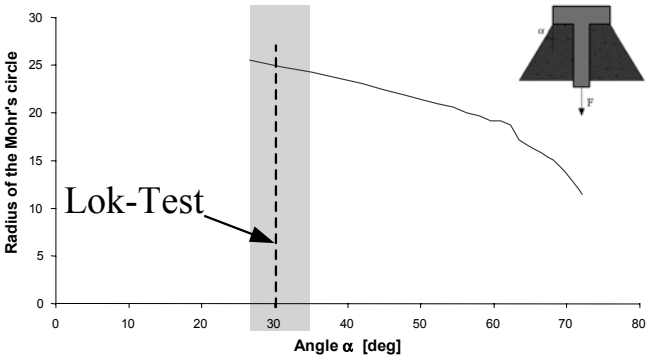

Figure 39 : Mohr radius at crack initiation for variable value of the apex angle

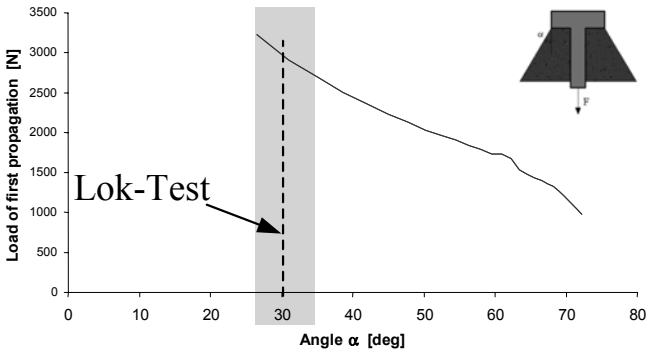

Figure 41 : Load at crack initiation for variable value of apex angle

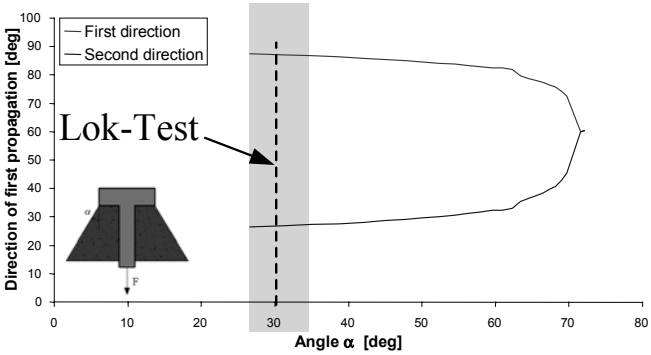

Figure 40 : Propagation directions at crack initiation for variable value of the apex angle

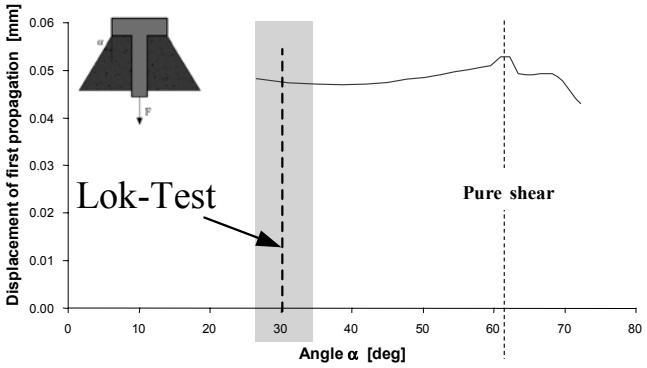

Figure 42 : Displacement at crack initiation for variable value of the apex angle

5.5 Crack propagation analysis

A step-wise analysis of crack propagation has been performed for the pullout geometry of the Lok-Test.

According to the discrete crack approach, a modification of the mesh is required at each step of the crack propagation process. The tool here adopted for crack geometry updating and remeshing is described in Ferretti (2003).

The numerical crack path and the stress analysis predicted by the numerical model are shown in Fig. 43 for four failure stages. In accordance with the experimental results (Fig. 2), the numerical direction of propagation changes at every stage. In particular, after a subvertical propagation the propagation direction changes abruptly and the crack propagates towards the counterpressure ring. The intra-element propagation technique and reduction of the mesh size near the crack tip allow the crack path to be accurately predicted.

From the stress and principal directions analysis in Fig. 43 one can conclude that the static scheme of the resistant structure changes at each propagation step. In particular, at first the resistant structure is subjected to compressive stresses in the disk-counterpressure ring direction. For this stage, the principal stresses are nonuniform and the principal directions are not parallel to each other, as in the linear-elastic finite element analysis of Stone and Carino (1984). As the crack propagates, bending actions superimpose to the compressive stresses. As a consequence, the transferring zone of compressive stresses becomes thinner and thinner, and the non-uniform stress behavior is enhanced. The comparison of a neutral axis in the concrete to be extracted arises simultaneously to the radical changing in the crack propagation direction. In the stress analysis for the third stage of Fig. 43, changing of the crack propagation direction and comparison of a tension zone near the stem are well recognizable. Dur-

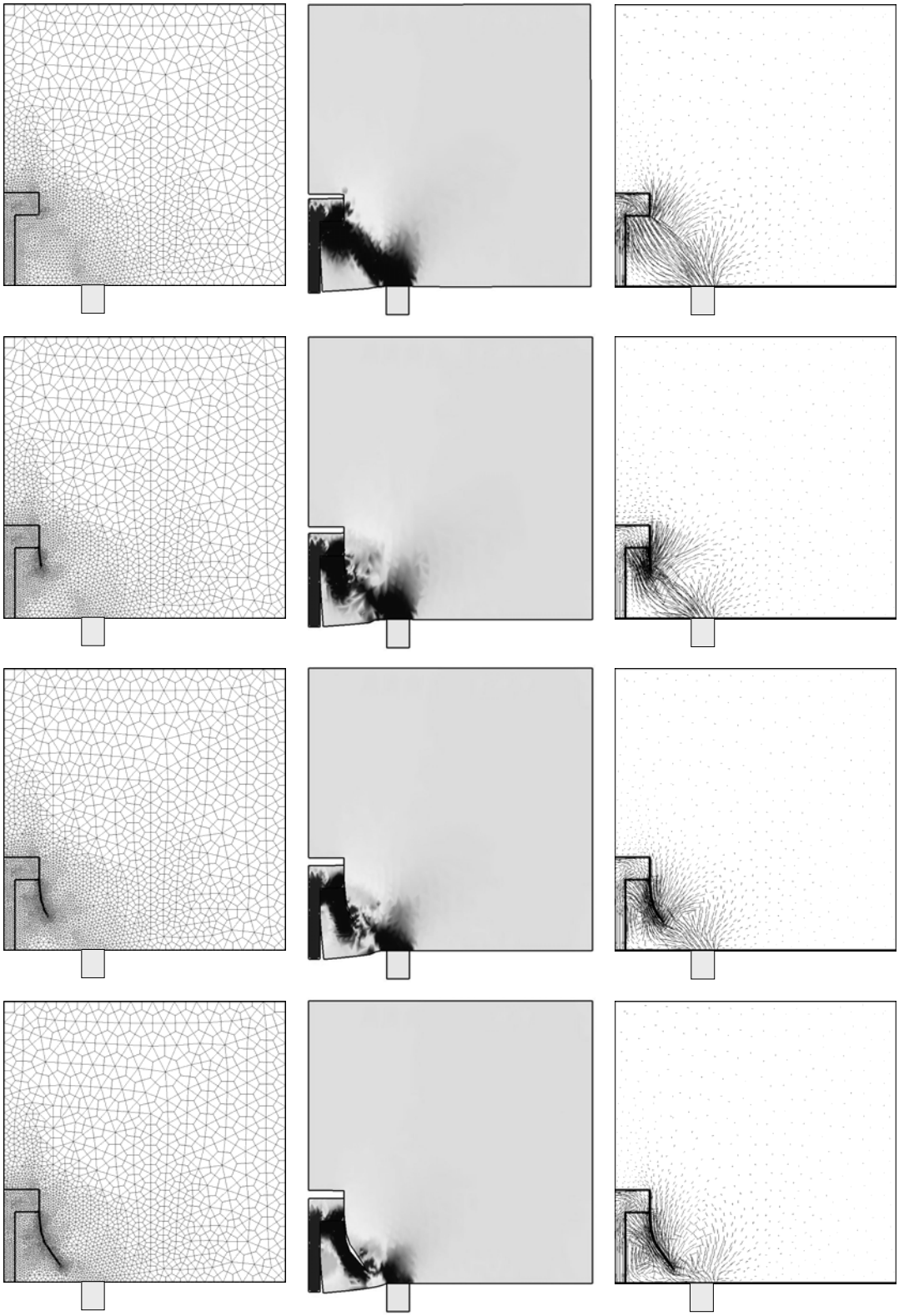

Figure 43 : Mesh, stress and strain analysis for four failure stages (geometry of Lok-Test)

ing the latter stages of crack propagation the bending actions become dominant. It can than be concluded that crack propagation also involves progressive bending of the compressed concrete within the concrete to be extracted. This result agrees with the plastic-fracture finite element analysis of Yener (1994).

The third stage of Fig. 43 also shows a modification of the stress field in front of the crack tip. In particular, a tensile state of stress with principal direction perpendicular to the crack last edge is well recognizable. Since the crack direction will remain unchanged from this moment forth, it is reasonable to conclude that the tensile state of stress contributes to crack propagation in this last phase of the pullout test. Also opening of the crack edges behind the crack tip confirms this assumption (Fig. 43, deformed configuration of third stage).

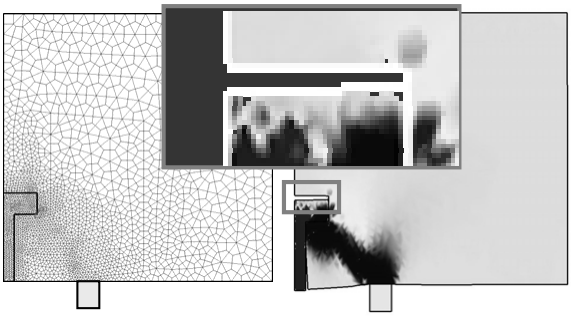

Figure 44 : Details of the deformed configuration above the disk shortly before crack initiation

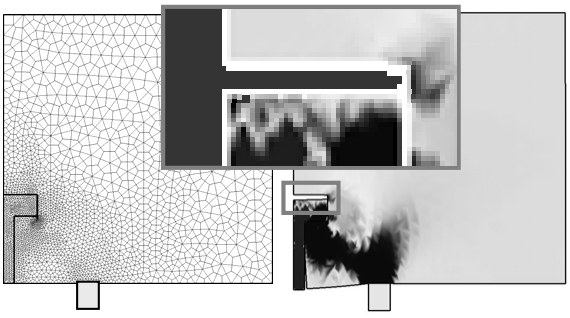

Figure 45 : Details of the deformed configuration above the disk soon after crack initiation

In Fig. 44, the zoom of the steel disk deformation is provided at the upper steel-concrete interface, soon before the crack starts to propagate. As in Yener (1994), the steel disk bends pronouncedly, while the concrete is quite undeformed.

At this point, the concrete within the eventual failure surface is compressed in the insert-support ring direction. When the crack activates, the decrease of concrete stiffness under the steel disk due to crack propagation leads to a steel disk bending close to zero (Fig. 45). From this moment forth, the stiffness of the steel disk can be assumed to be infinite.

With reference to the node numeration in Fig. 9, the followings are further similarities between the present and Yener's analysis:-

- The vertical downward displacement of node 1, δ_1 is always greater than that of node 2, δ_2.
- Both δ_1 and δ_2 are always greater than δ_4.
- The concrete to be extracted pushes against the main body of the concrete near the support ring and against the steel stem near point 1.
- High compressive interacion exists between the stem and the concrete direcly below the steel disk in the vicinity of the periphery near to point 1.

6 Conclusions

A CM code has been used here both for crack initiation and crack propagation analysis in the pullout test modeling. Several ratios between the internal diameter of the counterpressure ring and the rod length have been taken into account for the crack initiation analysis. The crack propagation analysis has been performed for the geometry of the Lok-Test. The adopted CM code combines nodal relaxation, intra-element propagation and remeshing. It also permits the mesh dimensions to be refined at specific locations, so as to improve the accuracy of the solution. The mesh generator ability to operate on multiple domains has been used to provide the evolving stress field both in the steel insert and concrete specimen. Finally, the code automatically estimates which part of the boundary is subjected to Mode I loading, and which part is subjected to Mode II loading. Consequently, no a-priori assumptions are needed on the steel-concrete interaction. The computation is then performed on the whole domain, without having to reduce the analysis on the

equilibrium condition of the extracted concrete. The simulation is displacement-controlled. The agreement between CM results and results of previous FEM analysis further states that the CM can give good predictions for fracture mechanics problems. Also the experimental results are well reproduced. The step-wise analysis of the state of stress allows us to describe the progressive failure of the concrete medium. It was found that the crack initiation mechanism depends upon the ratio between the internal diameter of the counterpressure ring and the rod length. A changing in the crack initiation mechanism from shear-compression to shear-tension was found to occur for the angle α equal to about 63°. Moreover, the crack propagation mechanism changes as the crack propagates. At first, the concrete between the steel disk and the conterpressure ring is compressed in the disk-ring direction. Subsequently, bending actions develop in the concrete fragment to be extracted. They become more and more relevant with the evolving of the failure process and a neutral axis arises in the concrete fragment. Compressive interactions between steel rod and concrete specimen and the punching effect at the disk-concrete interface cause the neutral axis to intersect the rod-concrete interface, never arriving at the disk-concrete interface. The direction of the neutral axis is more or less parallel to the crack direction. The comparison of the neutral axis seems to be correlated to the abrupt change of the crack propagation direction, also experimentally observed. From the moment in which the crack direction changes on, a tensile state of stress develops in front of the crack tip. It may then be reasonable to assume that tensile strength of the concrete has some kind of indirect influence on the pullout strength. It can be concluded that it may be not appropriate to describe the complex state of stress induced in pullout test by a uniaxial mode of failure. As in the conclusions of the linear-elastic finite element analysis of Stone and Carino, it can also be asserted that an alternative explanation needs to be found for the experimentally observed close correlation between compressive and pullout strength.

The analysis of the stress field provides a detailed description of the stress redistribution with the crack propagation. It seems then that the CM code is able to provide a substantial contribution to the comprehension of the physical mechanism of failure in pullout tests.

The analysis performed has been carried out by following only one of the two experimentally observed crack paths. Numerical results can improve if the second crack path is modeled as well. Further studies are currently being undertaken to activate the second propagation and study the mutual influence between the two cracks. Moreover, an extension of the code in such a way as to take into account the friction between the nodes lying on the crack edges is being studied at the present time. Finally, also combination of concrete crushing and concrete cracking is under study at the moment, so as to derive the complete load-displacement diagram in pullout tests.

Acknowledgement: All the results here presented are part of the CIMEST Scientific Research on the Identification of Materials and Structures – DISTART – Faculty of Engineering –Alma Mater of Bologna.

References

Atluri, S. N.; Shen, S. (2002): *The Meshless Local Petrov-Galerkin Method*, Tech Science Press.

Atluri, S. N.; Shen, S. (2002): The Meshless Local Petrov-Galerkin (MLPG) Method: A Simple \ & Less-costly Alternative to the Finite Element and Boundary Element Methods. *CMES: Computer Modeling in Engineering & Sciences*, vol. 3, No. 1, pp. 11-52.

Atluri, S. N.; Zhu, T. (1998): A New Meshless Local Petrov-Galerkin (MLPG) Approach in Computational Mechanics. *Comput Mech*, vol. 22, pp. 117-127.

Ballarini, R.; Shah, S. P.; Keer, L. M. (1986): Failure Characteristics of Short Anchor Bolts Embedded in a Brittle Material. *Proceedings*, *Royal Society of London*, A404, pp. 35-54.

Belytschko, T.; Lu, Y. Y.; Gu, L. (1994): Element Free Galerkin Methods. *Int J Num Meth Engrg*, vol. 37, pp. 229-256.

Bergan, P. G. (1985): Record of the Discussions on Numerical Modeling. *Mechanics of Geomaterials and Concrete*, Z. P. Bažant ed.

Bishop, A. W.; Green, G. E. (1965): The Influence of end Restraint on the Compression Strength of a Cohesionless Soil. *Géotechnique*, vol. 15, pp. 243-266.

Bocca, P. (1984): The application of Pull-Out Test to High Strength Concrete Estimation. *Matériaux et Constructions*, vol. 17, No. 99, pp. 211-216.

Bocca, P.; Carpinteri, A.; Valente, S. (1989): Evaluation of Concrete Fracture Energy Through a Pull-Out

Testing Procedure. *Fracture of Concrete and Rock*, pp. 347-356.

Chabowski, A. J.; Bryden-Smith, D. W. (1980): Assessing the Strength of Concrete of In-Situ Portland Cement Concrete by Internal Fracture Tests. *Mag Concrete Res*, vol. 32, No. 112, pp. 164-172.

Deman, F. (1975): Achsensymetrische Spannungs-und Verformungsfelder in trockenem Sand. *Dissertation, University of Karlsruhe*, No. 62.

Domone, P. L.; Castro, P. F. (1987): An Expanding Sleeve Test for In-Situ Concrete and Mortar Strength Evaluation. *Proc. Structural Faults and Repairs 87*.

Dresher, A.; Vardoulakis, I. (1982): Geometric Softening in Triaxial Tests on Granular Material. Geotechnique, vol. 32, No. 4, pp. 291-303.

Ferretti, E. (2003): Crack Propagation Modeling by Remeshing Using the Cell Method (CM). *CMES: Computer Modeling in Engineering & Sciences*, vol. 4, No. 1, pp. 51-72.

Ferretti, E.; Di Leo, A. (2003): Modelling of Compressive Tests on FRP Wrapped Concrete Cylinders through a Novel Triaxial Concrete Constitutive Law. *SITA*, vol. 5, pp. 20-43.

Ferretti, E.; Bastianini, F. (2002): Identification of the Local $\sigma_{eff} - \varepsilon_{eff}$ Law for Concrete under Uniaxial Monotone Compression, *Proc ABDM*, full text on CD-ROM (16 pp.).

Ferretti, E.; Viola, E.; Di Leo, A. (2002-a): Crack Trajectory in Tensioned Concrete Plates using the Cell Method. *Proc WCCM V*, full text on CD-ROM (10 pp.).

Ferretti, E.; Viola, E.; Di Leo, A. (2002-b): Limiting Load in Concrete Plates with Cracks: a Cell Method (CM)-Based Calculation. *Proc ASEM'02*, full text on CD-ROM (8 pp.).

Ferretti, E. (2001): *Modellazione del Comportamento del Solido Cilindrico Compresso*. Ph.D. Thesis, University of Lecce, Italy.

George, P. L.; (1995): Automatic mesh generator using the Delaunay Voronoi principle. *Surv Math Ind*, pp. 239-247.

Hadamard, J. (1903): *Leçons sur la Propagation des Ondes – Chapter VI*, Paris, France.

Har, J. (1998): *A New Scalable Parallel Finite Element Approach for Contact-Impact Problems*. Ph.D. Thesis, Georgia Institute of Technology, Atlanta.

Hegemier, G. A.; Read, H. E. (1983): Some Comments on Strain-Softening. *DARPA-NSF Workshop*, 19 pp.

Hellier, A. K; Sansalone, M; Carino, N. J; Stone, W. C.; Ingraffea, A. R. (1987): Finite-element Analysis of the Pullout Test Using a Nonlinear Discrete Cracking Approach. *Journal of Cement, Concrete and Aggregates*, vol. 9, No. 1, pp. 20-29.

Hettler, A. (1981): Verschiebungen starrer und elastischer Grundungskörper in Sand bei monotonen und zyklischer Belastung. *Dissertation, University of Karlsruhe*.

Hudson, J. A.; Brown, E. T.; Fairhurst, C. (1971): Shape of the Complete Stress-Strain Curve for Rock. *Proc. 13th Symposium on Rock Mechanics*.

Jensen, B. C.; Bræstrup, M. W. (1976): Lok-Tests Determine the Compressive Strength of Concrete. *Nordisk Betong (Journal of the Nordic Concrete Federation)*, No. 2, pp. 9-11.

Kim, H. G.; Atluri, S. N. (2000) Arbitrary Placements of Secondary Nodes, and Error Control, in the Meshless Local Petrov-Galerkin (MLPG) Method. *CMES: Computer Modeling in Engineering & Sciences*, vol. 1, No. 3, pp. 11-32.

Kirkpatrick, W. M.; Belshaw, D. J. (1968): On the Interpretation of the Triaxial Test. Géotechnique, Vol. 18, No. 3, pp. 336-350.

Kierkegaard-Hansen, P. (1975): Lok-Strength. *Nordisk Betong (Journal of the Nordic Concrete Federation)*, No. 3, pp. 19-28.

Krenchel, H.; Bickley, J. A. (1985): Pullout Testing of Concrete. Historical Background and Scientific Level Today. *Nordic Concrete Research*, Publ. No. 6, The Nordic Concrete Federation.

Mailhot, G.; Bisaillon, G.; Carette, G. G.; Malhotra, V. M. (1979): In-Place Concrete Strength: New Pullout Methods. *ACI Journal*, vol. 76, No. 12, pp. 1267-1282.

Nikishkov, G. P.; Park, J. H.; Atluri, S. N. (2001): SGBEM-FEM Alternating Method for Analysing 3D Non-planar Cracks and Their Growth in Structural Components. *CMES: Computer Modeling in Engineering & Sciences*, vol.2, No. 3, pp. 401-422.

Ottosen, N. S. (1981): Nonlinear Finite Element Analysis of Pull-Out Test. *Journal of the Structural Division*, vol. 107, No. ST4, pp. 591-603.

Papadopoulos, P.; Jones, R. E.; Solberg, J. (1995): A Novel Finite Element Formulation for Frictionless Con-

tact Problems. *Int J Num Meth Engrg*, vol. 38, pp. 2603-2617.

Petersen, C. G. (1984): Lok-Test and Capo-Test Development and Their Applications. *Proceedings, Institution of Civil Engineering*, Part I, 76, pp. 539-549.

Petersen, C. G. (1984): Lok-Test and Capo-Test Pullout Testing, Twenty Years Experience. *Proc. Non-Destructive Testing in Civil Engineering Conference*, pp. 1-10.

Rashid, M. M. (1998): The Arbitrary Local Mesh Replacement Method: an Alternative to Remeshing for Crack Propagation Analysis. *Comput Methods Appl Mech Engrg*, vol. 154, pp. 133-150.

Sandler, I.; Wright, J. P. (1983): Summary of Strain-Softening. *DARPA-NSF Workshop*.

Stone, W. C.; Carino, N. J. (1983): Deformation and Failure in Large-Scale Pullout Tests. *ACI Journal*, vol. 80, No. 6, pp. 501-513.

Stone, W. C.; Carino, N. J. (1984): Comparison of Analytical with experimental Internal Strain Distribution for the Pullout Test. *ACI Journal*, vol. 81, No. 1, pp. 3-12.

Tonti, E., (2001): A Direct Discrete Formulation of Field Laws: the Cell Method. *CMES: Computer Modeling in Engineering & Sciences*, vol.2, No. 2, pp. 237-258.

Wu, F. H.; Freud, L. B. (1983): Deformation Trapping due to Thermoplastic Instability in One-Dimensional Wave Propagation. *Report MRL-E-145*, Brown University, Providence, RI, USA.

Tradegard, A.; Nilsson F.; Ostlund S. (1998): FEM-Remeshing Technique Applied to Crack Growth Problems. *Comput Method Appl M*, vol. 160, pp. 115-131.

Yener, M. (1994): Overview and Progressive Finite Element Analysis of Pullout Tests. *ACI Structural Journal*, vol. 91, No. 1, pp. 49-58.

Wrobel, L. C.; Aliabadi, M. H. (2002): *The Boundary Element Method*, Wiley-Vch.

Yener, M.; Chen, W. F. (1984): On In-Place Strength of Concrete and Pullout tests. *Journal of Cement, Concrete, and Aggregates*, vol. 6, No. 2, pp. 90-99.

Zhong, Z. H. (1993): Finite Element Procedures for Contact-Impact Problems. Oxford/New York/Tokyo, 372 pp., Book review: *Appl Mech Rev*, vol. 48, No. 5, 1995, 5R4 (written by M. Okrouhlik).